



Nano-roughness in gold revealed from X-ray signature

J.L. Glover^a, C.T. Chantler^{a,*}, Martin D. de Jonge^b

^a School of Physics, University of Melbourne, Australia

^b Australian Synchrotron, Clayton, Victoria, 3168, Australia

ARTICLE INFO

Article history:

Received 21 January 2009

Accepted 22 January 2009

Available online 31 January 2009

Communicated by V.M. Agranovich

PACS:

78.70.Dm

32.80.Aa

47.54.Jk

68.35.bd

68.35.Ct

Keywords:

Roughness

Materials characterisation

Synchrotron radiation

ABSTRACT

We present a new method for investigating roughness for surface structure and internal inhomogeneity down to the nano-scale for thin, nano-structured and opaque materials. The method uses careful measurements of the X-ray mass-attenuation coefficient and is applied to measure the magnitude of the roughness of gold foils. The technique is unique, providing insight into both surface and internal roughness. We show that moments of the distribution function of surface and internal structure can be investigated using this method, and discuss observable signatures. The approach is non-destructive and very sensitive as a local in situ measurement and as a diagnostic for accurate characterisation.

© 2009 Elsevier B.V. All rights reserved.

1. Introduction

We report a new technique for investigating roughness from the mm to nm scale. This non-destructive technique determines the roughness of a sample by careful measurement of the X-ray mass-attenuation coefficient. The technique provides insight into both surface and internal roughness. It can be applied to a wide class of samples and can be useful in nano-fabrication, surface-science, high-precision optics and in many other areas requiring non-destructive characterisation of internal or surface roughness.

The roughness of a sample can be divided into two components: surface roughness and internal inhomogeneity. Surface roughness is a measure of the small-scale variability in surface height across a sample and is widely studied using numerous existing techniques including stylus [1] and optical profilometry [2], atomic force microscopy (AFM) and scanning tunnelling microscopy (STM) [1,3], transmission electron microscopy (TEM) and scanning electron microscopy (SEM) [4,5] and X-ray reflection [6].

Internal inhomogeneity (which will be referred to as internal roughness) is manifest in the density non-uniformities and voids within the bulk of the sample. X-rays are extremely penetrative and can interrogate the bulk of a sample, allowing the measure-

ment of roughness not only at the surface but also within the bulk. Hence our technique can provide unique insight into internal roughness and open exciting new research opportunities, including studies of nano-structures in cement [7], energy conversion devices [8], and the effects of nano-scale roughness which lead to effects on stresses [9].

Our technique can be summarised as follows. Measurements of the X-ray mass-attenuation coefficient are made over a range of energies on the sample of unknown roughness that is being investigated. Measurements are also made on a set of thicker reference samples of low roughness. The attenuation of the unknown sample is compared to that of the reference samples and the difference is calculated. The magnitude of the roughness can then be determined based on the size and form of this difference.

2. Measuring mass-attenuation coefficients

The X-ray mass-attenuation coefficient [$\frac{\mu}{\rho}$] quantifies the extent to which a material absorbs and scatters X-rays. In order to measure the mass-attenuation coefficient accurately, we use the X-ray extended range technique (XERT) [10–12], which can correct for a wide range of systematic errors including scattering [13], fluorescence [14], harmonics [15], bandwidth [16], and the attenuation of the ion-chambers and air-path. The XERT has produced the most accurate measurements of the mass-attenuation coefficient in the

* Corresponding author.

E-mail address: chantler@ph.unimelb.edu.au (C.T. Chantler).

literature [17], and this high accuracy now allows us to detect and measure roughness.

2.1. The effect of roughness on the mass-attenuation coefficient

A new roughness parameter is needed to reflect the extension of scope provided by this technique. We define roughness as the variability in $[\rho t]$ seen by the X-ray beam passing through the sample; $[\rho t]$ is the integrated column density and quantifies how much matter lies along the path of the X-ray beam

$$[\rho t] = \int_P \rho(x) dx, \quad (1)$$

where P is the path of the X-ray beam and $\rho(x)$ is the density of the sample at the point x . An X-ray beam has a finite size and different parts of the beam take different parallel paths through the sample. When the integrated column density along these paths is variable then the sample appears rough.

We define the magnitude of the roughness using the standard deviation of the integrated column-density $\sigma_{[\rho t]}$

$$\sigma_{[\rho t]}^2 = \frac{1}{A} \iint_S ([\rho t]_{(x,y)} - [\rho t]_{ave})^2 dS, \quad (2)$$

where S corresponds to the region of the sample being illuminated by the beam (with an area of A) assuming the foil is oriented perpendicular to the beam. $\sigma_{[\rho t]}$ is the most natural roughness parameter to use in X-ray absorption measurements since it takes into account surface roughness and internal roughness.

Consider an X-ray beam incident onto a rough metal foil: the measured mass-attenuation coefficient must take into account the distribution of $[\rho t]$ across the area (A) of the X-ray beam B . Assuming uniform incident intensity across the beam, roughness changes the measured mass-attenuation coefficient $[\frac{\mu}{\rho}]_m$

$$e^{-[\frac{\mu}{\rho}]_m [\rho t]} = \frac{1}{A} \int_B \exp\left\{-\left[\frac{\mu}{\rho}\right][\rho t]_{(x,y)}\right\} dB. \quad (3)$$

Here, $[\rho t]_{(x,y)}$ is the integrated column density at position (x, y) within the area of the sample illuminated by the X-ray beam B . By performing a Taylor expansion on the exponential term about $[\frac{\mu}{\rho}][\rho t]_{ave}$, the following equation can be derived for the measured discrepancy of the mass-attenuation coefficient $\Delta_{[\frac{\mu}{\rho}]}$

$$\Delta_{[\frac{\mu}{\rho}]} = \frac{-1}{[\rho t]_{ave}} \log\left(1 - \frac{[\frac{\mu}{\rho}]_m^2 \sigma_{[\rho t]}^2}{2}\right). \quad (4)$$

This equation describes how roughness alters the measured mass-attenuation coefficient and shows us that roughness produces a clear signature with a distinct dependence on the mass-attenuation coefficient.

Eq. (4) holds for all values of the mass-attenuation coefficient. If one were to measure $\Delta_{[\frac{\mu}{\rho}]}$ over a range of values of the mass-attenuation coefficient then the two remaining parameters in the equation ($\sigma_{[\rho t]}$ and $[\rho t]_{ave}$) could be determined by fitting the equation to the data. Measuring $\Delta_{[\frac{\mu}{\rho}]}$ over a wider range of attenuation values allows the roughness to be characterised robustly and accurately.

3. Experimental results

Measurements of the mass-attenuation coefficient of five gold foils were performed at bending-magnet beamline 20B of the Photon Factory synchrotron in Japan using X-rays between 14 keV and 21 keV. The measured mass-attenuation coefficient of the four reference foils were consistent, but the 5 μm sample showed a clear

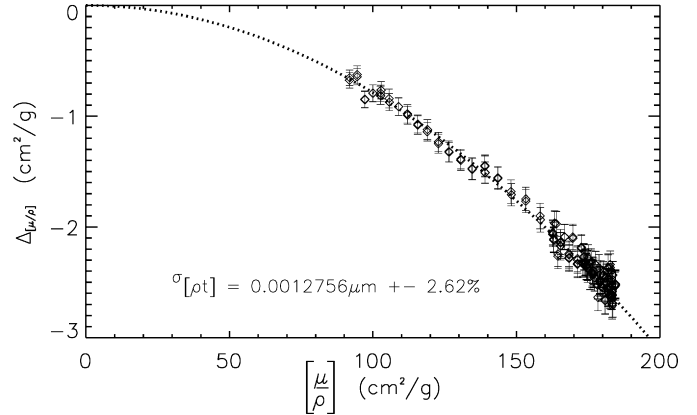


Fig. 1. The measured value of $\Delta_{[\frac{\mu}{\rho}]}$ along with error bars are plotted against $[\frac{\mu}{\rho}]$ for the rough 5 μm gold foil. The magnitude of the roughness was determined using a least-squares fitting procedure and a model based on Eq. (4); the results of the model are plotted as a dotted line. The experiment and the model are in excellent agreement.

residual signature. The discrepancy was seen across the entire energy range and is plotted in Fig. 1. It was caused by roughness and had a smooth dependence upon the mass-attenuation coefficient.

3.1. Determination of thickness and roughness

The roughness parameter must be determined simultaneously with $[\rho t]$, since the two variables are highly correlated (the correlation coefficient was 0.95 in this case). The effect of roughness on the 5 μm sample was modelled, and the magnitude of the roughness in that sample was fitted to be

$$\sigma_{[\rho t]_{5 \mu\text{m}}} = 0.001276 \text{ g/cm}^2 \pm 2.6\%. \quad (5)$$

The integrated column density of the (nominally) 5 μm sample was fitted to be:

$$[\rho t]_{5 \mu\text{m}} = 0.010287 \text{ g/cm}^2 \pm 0.067\%. \quad (6)$$

Assuming a density of 19.3 g/cm^3 for the gold foil yields a thickness of $t = 5.3301 \mu\text{m} \pm 0.0036 \mu\text{m}$, and a roughness of $\sigma_{[t]} = 661 \text{ nm} \pm 17 \text{ nm}$. The best-fit model of the discrepancy due to roughness is compared to experiment in Fig. 1. The agreement between the two is excellent.

4. Discussion

4.1. Surface and internal roughness

This determination of roughness takes into account surface and internal roughness. Internal roughness is not accessible using existing techniques, so it is useful to give it further consideration. We partition the sample into the lower surface S_1 , the upper surface S_2 , and the interior V . Now we can consider the contribution of each of these regions to the roughness parameter:

$$\sigma_{[\rho t]}^2 = \sigma_{S_1}^2 + \sigma_{S_2}^2 + \sigma_V^2 - 2\sigma_{S_1}\sigma_{S_2}r_{S_1,S_2} \quad (7)$$

$$+ 2\sigma_{S_1}\sigma_V r_{S_1,V} - 2\sigma_V\sigma_{S_2} r_{V,S_2}. \quad (8)$$

Here, σ_{S_1} represents the RMS roughness of the lower surface multiplied by the density and r_{S_1,S_2} represents the correlation coefficient between the two surfaces.

If we assume that the two surfaces and any voids are uncorrelated, then the equation reduces to

$$\sigma_{[\rho t]}^2 = \sigma_{S_1}^2 + \sigma_{S_2}^2 + \sigma_V^2. \quad (9)$$

This equation allows us to characterise the internal roughness σ_V by measuring the roughness of both surfaces using other X-ray or

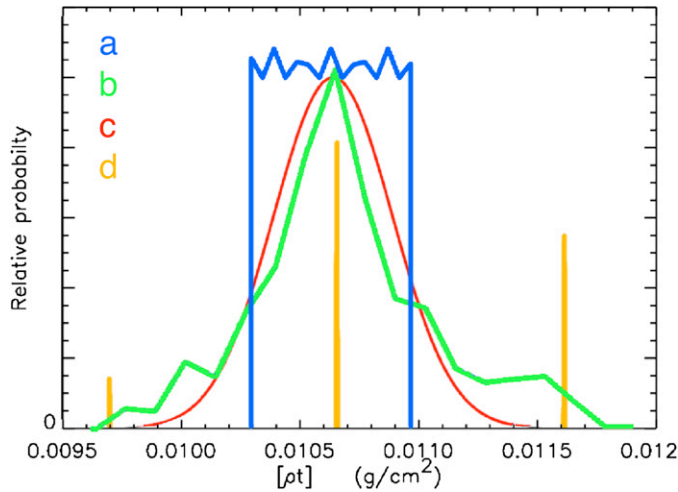


Fig. 2. Examples of four different causes and distributions of roughness. (a) A simple sawtooth surface typically produced by tooling or polishing defects [blue]; (b) A fractally generated rough surface [green]; (c) Normally distributed surface roughness with a distribution of internal voids requiring a technique such as that described here [red]; (d) This surface is an idealisation of the structure seen on the surface due to growth of crystal planes [ochre]. This type of surface has a height-distribution function consisting (ideally) of delta-functions. (For interpretation of the references to colour in this figure legend, the reader is referred to the web version of this Letter.)

profilometry methods. This information could be combined as a scaling parameter $\frac{\sigma_{z_1}^2 + \sigma_{z_2}^2}{\sigma_{[\rho t]}^2}$, which contains information about the internal structure of the sample. A value of unity for this parameter would indicate the sample had no significant internal roughness; a value of less than one would indicate the presence of internal voids and inhomogeneity. This scaling parameter could also be useful for investigating surface correlation. For example, a value greater than unity would indicate that the upper and lower surfaces of the sample have a correlated structure such as might result from rolling, extruding or tooling.

4.2. Surface-height profile and R_a

Another parameter used to represent surface roughness is R_a , the ‘average roughness’. R_a is one of the standard surface-texture parameters defined by the International Standards Organisation [18]. Given a surface S with surface area A and a surface-height distribution $Z(x, y)$, R_a is

$$R_a = \frac{1}{A} \iint_S |Z(x, y) - Z_{ave}| dS. \quad (10)$$

Measurements of R_a and $\sigma_{[\rho t]}$ can be combined to extract surface-profile information. By measuring R_a and $\sigma_{[\rho t]}$ for the same sample, one could discriminate between different surface-height distributions. Some examples of possible sample structures are given in Fig. 2 and the corresponding surface-height distributions are shown in Fig. 3; we can discriminate between these cases because each displays a different value of the ratio $(\rho R_a)/\sigma_{[\rho t]}$.

The values of the ratio of $\rho \times R_a$ to $\sigma_{[\rho t]}$ for the different distribution-functions are indicated in Table 1. The significant variation between the ratios for these distributions can probe the dominant cause of roughness in a sample and the higher moments of the thickness-distribution function. The value of this parameter provides a qualitative distinction between residual grooves or tooling defects (top-hat distribution) or a beautiful etched surface (possibly binomial) or a fractal fracture surface [19]. Additionally, if the ratio observed were much below the entries in Table 1, then

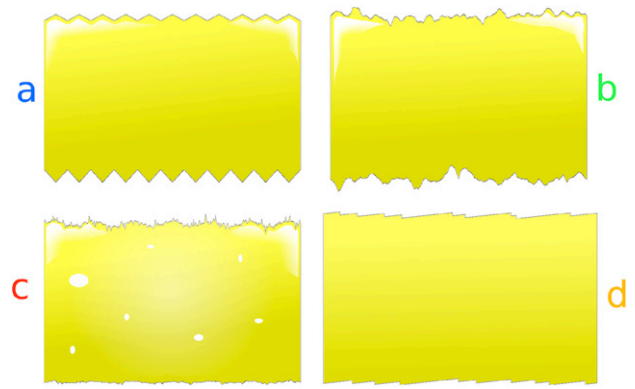


Fig. 3. Plots of the $[\rho t]$ distribution functions of the four samples shown in Fig. 2(a), (b), (c) and (d). The picture and corresponding graph are shown in the same colour. The two roughness parameters discussed (R_a and $\sigma_{[\rho t]}$) respond differently to different distributions.

Table 1

The value of $\rho R_a/\sigma_{[\rho t]}$ for several surface-height distribution-functions, including a top-hat, fractal, Gaussian and binomial (examples of how these surfaces might look can be seen in Fig. 2(a), 2(b), 2(c) and 2(d) respectively). The presence of voids will lower this ratio. Determining this ratio can qualitatively assess the dominant cause of roughness, and can demonstrate the significance of voids in a particular sample.

	Top-hat	Fractal	Gaussian	Binomial
$\rho R_a/\sigma_{[\rho t]}$	0.866	0.650	0.798	0.709

this would imply that voids were a dominant source of sample non-uniformity.

Obtaining this ratio permits more detailed characterisation of the distribution function across a range of roughness scales which are not easily accessible via other techniques. Importantly the second moment is usually unavailable, and this combined approach can access this effectively and may lead to improvements in metallurgical and industrial processing applications.

4.3. Possible limits of validity of the technique

We have determined the roughness of a particular gold sample to be $661 \text{ nm} \pm 17 \text{ nm}$, but what would be the lower limit of roughness measurable using this technique? Eq. (4) allows us to estimate this. If we were to take measurements at lower energies, say 4–7 keV, where the mass-attenuation coefficient is 3–10 times larger than it is in the 14–19 keV range, we would be able to observe significantly smaller roughness parameters. At these energies a roughness of 114 nm for a $1 \mu\text{m}$ sample should produce a signal just as clear as that seen in our measurements. The calculated discrepancy indicates that this technique should be capable of measuring roughness to below 50 nm. If the experiment were performed at a 3rd-generation synchrotron (e.g. an undulator), then increased flux would allow the quantification of even smaller roughnesses—below 30 nm.

An interesting extension of this technique could involve varying the X-ray beam-size. This would allow determination of the characteristic length scales of the roughness variation. It would also provide an opportunity to investigate the fractal dimension of the sample [20–22].

4.4. Applications

This technique can be applied to characterise a wide range of materials and will be useful in a variety research fields. It can be implemented using any X-ray source that can provide multiple energies (e.g. laboratory X-ray tubes). If equipment were set up with this technique in mind then a full roughness characterisation could be extremely rapid.

There are numerous possible applications of this technique in the area of nano-circuitry and materials analysis. For example, one could diagnose a poor connection in a gold-coated silicon chip by identifying areas of roughness within the gold substrate. Equally, a nanofabricated layer can be checked for voids or smoothness. This technique is applicable in any area of nanofabrication and can provide information about surface and internal roughness that is not accessible with existing roughness characterisation methods.

5. Conclusion

In summary, we have presented a new technique and applied it to measure the roughness of gold foils down to the nano-scale. It is the first roughness-characterisation technique that enables the investigation of both surface and internal roughness. The technique is non-destructive and works equally well over large and small measurement areas. X-ray absorption roughness measurement shows great potential, and with further optimisation, improvements in roughness detectability of orders of magnitude should be possible. In particular, roughness scales from millimetres down to 30–50 nm should be accessible with this approach. In the field of roughness, we have just scratched the surface!

References

- [1] C.Y. Poon, B. Bhushan, *Wear* 190 (1995) 76.
- [2] J.M. Bennett, *Meas. Sci. Technol.* 3 (1992) 1119.
- [3] G. Binnig, C.F. Quate, C. Gerber, *Phys. Rev. Lett.* 56 (1986) 930.
- [4] M. Chládek, V. Valvoda, C. Dörner, C. Holý, J. Grim, *Appl. Phys. Lett.* 69 (1996) 1318.
- [5] P. Schwander, C. Kisielowski, M. Seibt, F.H. Baumann, Y. Kim, A. Ourmazd, *Phys. Rev. Lett.* 71 (1993) 4150.
- [6] E. Spiller, D. Stearns, M. Krumrey, *J. Appl. Phys.* 74 (1993) 107.
- [7] A.J. Allen, J.J. Thomas, H.M. Jennings, *Nature Mater.* 6 (2007) 311.
- [8] A.S. Aricò, P. Bruce, B. Scrosati, J.-M. Tarascon, W. van Schalkwijk, *Nature Mater.* 4 (2005) 366.
- [9] B. Luan, M.O. Robbins, *Nature* 435 (2005) 929.
- [10] C.T. Chantler, C.Q. Tran, D. Paterson, D. Cookson, Z. Barnea, *Phys. Lett. A* 286 (2001) 338.
- [11] C.Q. Tran, C.T. Chantler, Z. Barnea, *Phys. Rev. Lett.* 90 (2003) 257401.
- [12] M. de Jonge, C. Tran, C. Chantler, Z. Barnea, B. Dhal, D. Paterson, E. Kanter, S. Southworth, L. Young, M. Beno, et al., *Phys. Rev. A* 75 (2007).
- [13] C.T. Chantler, C.Q. Tran, D. Paterson, Z. Barnea, D.J. Cookson, *Rad. Phys. Chem.* 61 (2001) 347.
- [14] C.Q. Tran, M.D. de Jonge, Z. Barnea, C.T. Chantler, *J. Phys. B* 37 (2004) 3163.
- [15] C.Q. Tran, Z. Barnea, M.D. de Jonge, B.B. Dhal, D. Paterson, D.J. Cookson, C.T. Chantler, *X-Ray Spectrometry* 32 (2003) 69.
- [16] M.D. de Jonge, Z. Barnea, C.Q. Tran, C.T. Chantler, *Phys. Rev. A* 69 (2004) 022717.
- [17] M.D. de Jonge, C.Q. Tran, C.T. Chantler, Z. Barnea, B.B. Dhal, D.J. Cookson, W.-K. Lee, A. Mashayekhi, *Phys. Rev. A* 71 (2005) 032702.
- [18] ISO, *Geometrical Product Specifications – Surface Texture* (2005), ISO 4287, 1997, Section 4.2.1.
- [19] B.B. Mandelbrot, D.E. Passoja, A.J. Paullay, *Nature* 308 (1984) 721.
- [20] J. Krim, I. Heyvaert, C. van Haesendonck, Y. Bruynseraede, *Phys. Rev. Lett.* 70 (1993) 57.
- [21] E.L. Church, *Appl. Opt.* 27 (1988) 1518.
- [22] W. Ehrenberg, *J. Opt. Soc. Am.* (1917–1983) 39 (1949) 741.